

THE INITIAL-FINAL MASS RELATIONSHIP: SPECTROSCOPY OF WHITE DWARFS IN NGC 2099 (M37)¹JASONJOT SINGH KALIRAI², HARVEY B. RICHER², DAVID REITZEL³, BRAD M. S. HANSEN^{3,4}, R. MICHAEL RICH³, GREGORY G. FAHLMAN⁵, BRAD K. GIBSON⁶, & TED VON HIPPEL⁷

ABSTRACT

We present new observations of very faint white dwarfs (WDs) in the rich open star cluster NGC 2099 (M37). Following deep, wide field imaging of the cluster using *CFHT*, we have now obtained spectroscopic observations of candidate WDs using both GMOS on *Gemini* and LRIS on *Keck*. Of our 24 WD candidates (all fainter than $V = 22.4$), 21 are spectroscopically confirmed to be bona fide WDs, 4-5 of which are most likely field objects. Fitting 18 of the 21 WD spectra with model atmospheres, we find that most WDs in this cluster are quite massive ($0.7\text{--}0.9 M_{\odot}$), as expected given the cluster's young age (650 Myr), and hence, high turn-off mass ($\sim 2.4 M_{\odot}$). We determine a new initial-final mass relationship and almost double the number of existing data points from previous studies. The results indicate that stars with initial masses between 2.8 and $3.4 M_{\odot}$ lose 70–75% of their mass through stellar evolution. For the first time, we find some evidence of a metallicity dependence on the initial-final mass relationship.

Subject headings: open clusters and associations: individual (NGC 2099) - techniques: spectroscopic - white dwarfs

1. INTRODUCTION

The initial-final mass relationship connects the mass of the final products of stellar evolution for intermediate mass stars, white dwarfs (WDs), to their progenitor mass. It is a required input for the determination of the ages and distances of globular clusters from modeling their WD cooling sequences (Hansen et al. 2004), for constraining chemical evolution in galaxies, for determining supernova rates (van den Bergh & Tammann 1991), and for understanding feedback processes and star formation in galaxies (e.g., Somerville & Primack 1999). Yet, despite its fundamental importance, this relation remains poorly constrained observationally.

The first attempt to map the relation was made by Weidemann (1977) by comparing theoretical models (e.g., Fusi-Pecci & Renzini 1976) of mass loss to the masses of a few WDs in both the Pleiades and Hyades star clusters. Since then most of the work has focused on using observations of WDs in young open star clus-

ters to provide empirical constraints on the relationship (Koester & Reimers 1981, 1985, 1993, 1996; Reimers & Koester 1982, 1989, 1994; Weidemann & Koester 1983; Weidemann 1987, Jeffries 1997). This effort, spanning almost two decades, is summarized in Weidemann (2000). The result is a monotonically increasing relationship based on about 20 data points, from observations of about a dozen star clusters.

A few recent studies, such as Claver et al. (2001) and Williams et al. (2004), have been successful in finding a half dozen WDs each in the Praesepe and NGC 2168 clusters. The synthesis of these data with the earlier studies results in an initial-final mass relationship displaying a fair amount of scatter. For example, depending on whose data one uses, initial mass stars of $3\text{--}4 M_{\odot}$ can produce WDs ranging anywhere from $0.65\text{--}0.8 M_{\odot}$. This result suggests that the relationship may have a stochastic component.

It is desirable to find a young, rich star cluster with a large number of WDs that can be spectroscopically studied. NGC 2099 is such a cluster, with 50 WD cluster candidates measured using imaging observations (Kalirai et al. 2001a). The cluster is very rich, containing over 4000 stars, and has a main-sequence turn-off of $\sim 2.4 M_{\odot}$. Its distance modulus is $(m-M)_V = 11.5$, and its reddening is $E(B-V) = 0.23$. In this *Letter*, we present a new WD initial-final mass relationship based on 18 WDs in NGC 2099. In the following *Letter*, we address the surprising result that all WDs in NGC 2099 (as well as those found in other young open clusters) are all DA spectral type (Kalirai et al. 2005).

2. OBSERVATIONS

Imaging and spectroscopic observations of NGC 2099 were obtained with the Canada-France-Hawaii (*CFH*), *Gemini North*, and *Keck I* telescopes. In our wide field *CFHT* imaging study (Kalirai et al. 2001a), we found ~ 67 WD candidates in the central $15'$ of NGC 2099. Based on comparisons between the cluster field and a blank field surrounding the cluster, we estimate the rate

¹ Based on observations with Gemini (run ID GN-2002B-Q-11) and Keck. Gemini is an international partnership managed by the Association of Universities for Research in Astronomy under a cooperative agreement with the National Science Foundation. The W. M. Keck Observatory, which is operated as a scientific partnership among the California Institute of Technology, the University of California, and NASA, was made possible by the generous financial support of the W. M. Keck Foundation.

² Department of Physics and Astronomy, 6224 Agricultural Road, University of British Columbia, Vancouver, BC, V6T 1Z4, Canada; jkalirai@astro.ubc.ca, richer@astro.ubc.ca.

³ Department of Physics and Astronomy, University of California at Los Angeles, Box 951547, Knudsen Hall, Los Angeles, CA 90095-1547; reitzel@astro.ucla.edu, hansen@astro.ucla.edu, rnr@astro.ucla.edu.

⁴ Alfred P. Sloan Research Fellow.

⁵ National Research Council of Canada, Herzberg Institute of Astrophysics, 5071 West Saanich Road, RR5, Victoria, BC V9E 2E7, Canada; greg.fahlman@nrc.gc.ca.

⁶ Centre for Astrophysics and Supercomputing, Swinburne University, P.O. Box 218, Hawthorn, VIC 3122, Australia; bgibson@swin.edu.au.

⁷ Department of Astronomy, University of Texas at Austin, RLM 15.308, C-1400, Austin TX 78712-1083; ted@astro.as.utexas.edu.

of field star contamination among our candidates to be $\sim 25\%$ (thus yielding 50 cluster WD candidates). We then plotted the locations of all of these faint-blue objects on the sky and obtained further observations of 3 smaller sub-fields in the cluster. These fields were chosen to maximize the number of WD candidates (all objects in the faint-blue end of the color-magnitude diagram [CMD] were treated as WD candidates). With *Gemini*, we imaged three 5.5×5.5 fields using the GMOS multi-object imaging/spectroscopic instrument (Murowinski et al. 2003). With *Keck*, we imaged the same three fields with the LRIS imaging/spectroscopic instrument that has a $5' \times 7'$ field of view (Oke et al. 1995). These imaging data were not significantly deeper than the original *CFHT* data and were only used to ensure astrometric accuracy for the spectroscopy.

Multi-object spectra were obtained for a single *Gemini* field, and for two of the *Keck* fields. The *Gemini* observations used the B600 grating, which simultaneously covers 2760 Å (centered at ~ 4700 Å). The data were binned by a factor of four in the spectral direction to improve the signal-to-noise ratio (S/N). The *Keck* observations use the 600/4000 grism (blue side) which simultaneously covers 2580 Å (centered at 4590 Å). For the *Gemini* field, we obtained 22 individual 1-hour exposures spread over 22 days, taken mostly at low air-masses (< 1.2) and good seeing ($\sim 0.8''$). For the *Keck* fields, we obtained 4 2000 s exposures in each of the two fields, also at sub-arcsecond seeing.

The *Gemini* spectroscopic data were reduced using the *Gemini* IRAF package, version 1.3. The *Keck* data were reduced using a set of python routines written by D. Kelson (2004, private communication; Kelson 2003). The individual exposures were bias subtracted, flat-fielded, cleaned for cosmic rays, wavelength calibrated, sky subtracted, extracted, combined, and flux calibrated (using bright standard stars) within each of these programs. Details of the steps involved in each of these procedures will be provided in a forthcoming paper (J. S. Kalirai et al. 2005, in preparation). The only major problem occurred for some of the *Keck* field 2 spectra, which were taken at high air-masses and so the bluest flux was lost as a result of atmospheric dispersion. Fortunately, two of the three stars that we were fitting from this field have also been observed in the higher S/N *Gemini* data.

In total, we obtained spectroscopy of 24 individual WD candidates in the field of NGC 2099 (3 of these stars turned out not to be WDs). Therefore, despite sampling only 14% of the total cluster area, we include almost 1/3 of the total WD population (cluster and field) given the careful positioning of the fields. This is therefore the largest individual star cluster WD sample that has ever been spectroscopically acquired. A CMD showing the locations of the NGC 2099 WDs is shown in Figure 1 (based on *CFHT* data). The 18 circles represent those objects that we were able to spectroscopically fit (see next section). Four of these, shown as open circles, represent those objects that have inconsistent theoretical magnitudes (from fitting the spectra) as compared to the observed magnitudes, assuming they are cluster members. Three WDs, which we could not fit with models, are shown as crosses. All of the complete spectra are shown in the companion *Letter* (Kalirai et al. 2005).

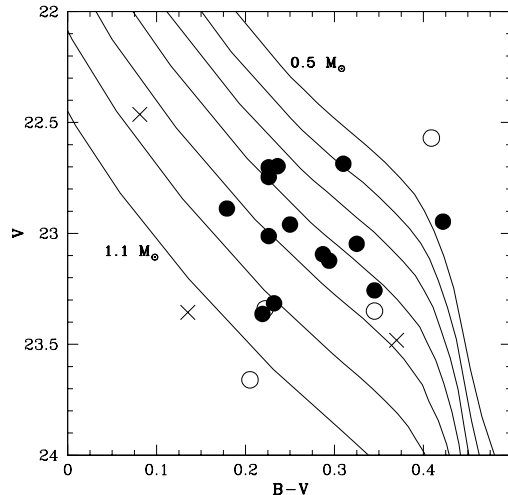


FIG. 1.— Faint-blue end of the CMD of NGC 2099 shown with all spectroscopically confirmed WDs in this work (21 objects - based on *CFHT* photometry). The 14 filled circles are those with consistent theoretical and observed magnitudes (assuming cluster membership), the 4 open circles have inconsistent theoretical magnitudes, and the 3 crosses are objects that we could not fit to spectral models. The model sequences represent WD cooling models (Fontaine, Brassard, & Bergeron 2001) at increments of $0.1 M_{\odot}$, with $0.5 M_{\odot}$ at the top and $1.1 M_{\odot}$ at the bottom.

3. ANALYSIS

Using the techniques described in Bergeron, Saffer, & Liebert (1992), we determine T_{eff} and $\log g$ for each WD. The line profiles are first normalized using two points on the continuum on either side of each absorption line. Therefore, the fit should not be affected by the flux calibration unless there is a strange “kink” or slope change at the location of a Balmer line. The fitting of the line shapes uses the nonlinear least-squares method of Levenberg-Marquardt (Press et al. 1986). The χ^2 statistic is calculated and minimized for combinations of T_{eff} and $\log g$, using normalized model line profiles of all absorption lines simultaneously. The resulting $1\text{-}\sigma$ errors in T_{eff} and $\log g$ were tested by simulating synthetic spectra with the same number of absorption lines, and similar S/Ns, and measuring the output parameters from fitting these spectra. These results are found to have errors slightly less than those in the true spectra (as expected given the small errors in flux calibration and other defects), and so we use the true spectra errors. Masses (M_f) and WD cooling ages (t_{cool}) are found by using the updated evolutionary models of Fontaine, Brassard, & Bergeron (2001) for thick hydrogen layers ($q(\text{H}) = M_{\text{H}}/M = 10^{-4}$) and helium layers of $q(\text{He}) = 10^{-2}$. The core is assumed to be a 50/50 C/O mix. In Figure 2 we present the model atmosphere fits for each WD.

The WD cooling age represents the time that each of these stars has spent traversing from the tip of the asymptotic giant branch (AGB) down to its present WD luminosity. We can now calculate the progenitor main-sequence lifetime (t_{ms} , the total lifetime of the star up to the tip of the AGB) assuming an age for the cluster. In Kalirai et al. (2001a), we fitted the NGC 2099 main-sequence to solar metallicity isochrones and determined

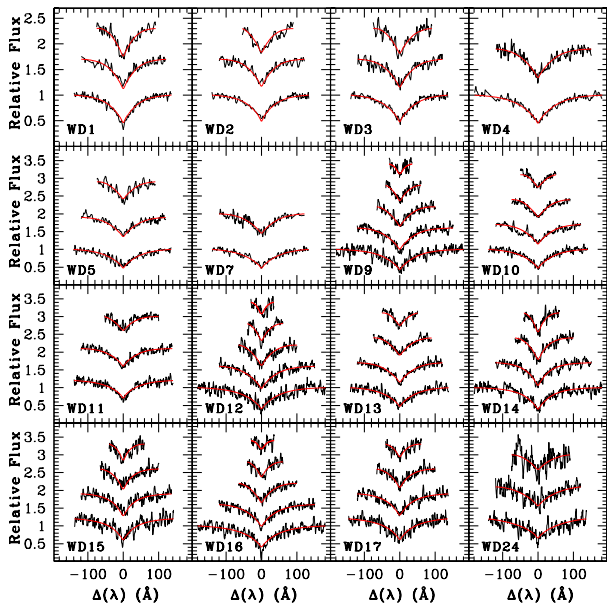


FIG. 2.— Spectroscopic fits (red) shown for the hydrogen Balmer lines of 16 WDs in NGC 2099. Within each panel, the lines are H_β (bottom), H_γ , H_δ , H_ϵ , and H_8 (top). The number of higher order lines varies depending on the spectral coverage of each star. The first six objects (WD1 – WD7) have the highest S/Ns and were obtained using *Gemini*. The remaining stars (*Keck* objects) have lower S/Ns but have bluer spectral coverage (hence the fitting of higher order lines). The identifications are the same as those in Kalirai et al. (2005), in which we present the full spectrum for all WDs. The corresponding T_{eff} , $\log g$, and M_f of these WDs are given in Table 1. The masses of two additional objects are measured as discussed in the text.

an age of 520 Myr. Recently, C. Deliyannis et al. (2004, private communication) have spectroscopically measured the cluster metallicity to be subsolar ($Z = 0.011 \pm 0.001$), and the reddening to be $E(B-V) = 0.23 \pm 0.01$, slightly larger than the value that we used. Using these parameters, the age of NGC 2099 is now calculated to be 650 Myr using the same Ventura et al. (1998) models and procedure as described in Kalirai et al. (2001a). We also derive similar ages using the Padova group (620 Myr - Girardi et al. 2000) and Yale-Yonsei isochrones (630 Myr - Yi et al. 2001) for this metallicity (J. S. Kalirai et al. 2005, in preparation).

The t_{ms} for each star is determined by subtracting the WD cooling ages (t_{cool}) from the cluster age (650 Myr). The initial progenitor masses (M_i) for the WDs are then calculated using the Hurley, Pols, & Tout (2000) models for $Z = 0.01$. For this metallicity, these models give very similar values to those derived from the Ventura et al. (1998) models. For these masses, a 100 Myr cluster age difference would only cause a $\sim 0.3 M_\odot$ initial mass difference (for 350 Myr lifetimes). This is a very small effect on our initial-final mass relationship, and therefore the results are not highly sensitive to the derived cluster age. Table 1 summarizes the derived parameters for each star, with $1-\sigma$ error bars. Also given are the theoretical magnitudes (from fitting the spectra) and the observed magnitudes [assuming $(m-M)_V = 11.5$ to NGC 2099].

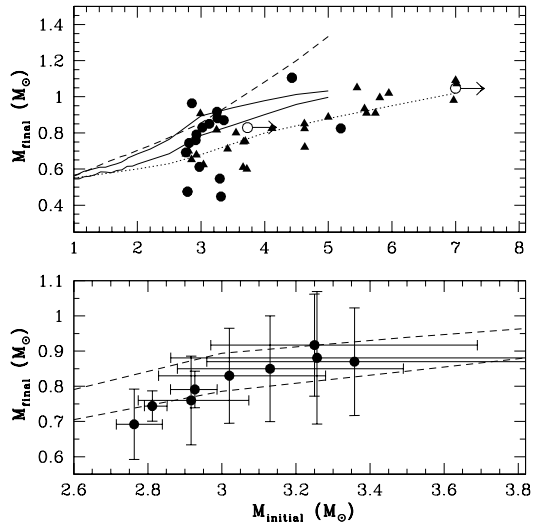


FIG. 3.— Top - WD initial-final mass relationship shown for the 18 WDs spectroscopically fitted in this work (circles) and all previous constraints (triangles). Also shown are several semi empirical and theoretical relations as discussed in the text. Bottom - Closer look at those WDs that form the tight sequence with $M_i = 2.8\text{--}3.4 M_\odot$ and are bound by the two Marigo (2001) theoretical relations.

4. THE INITIAL-FINAL MASS RELATIONSHIP

In Figure 3 (top) we present the initial-final mass relationship for the sixteen WDs in Figure 2 (filled circles), as well as two other objects, WD6 and WD21 (see Kalirai et al. 2005 for the spectra of these objects). For these two stars, we could not determine an accurate $\log g$ as a result of the spectra having too low S/Ns. However, the effective temperatures are well constrained, and therefore we derive the masses of the stars by combining this information with the luminosities (assuming they are cluster members). This gives the radius, which coupled with a mass-radius relation, gives the mass of the stars. The masses of these two stars, as well as their progenitor masses, are found to be in good agreement with others in the cluster (WD6 has $M_f = 0.92$ and $M_i = 3.25$, and WD21 has $M_f = 0.85$ and $M_i = 3.13$). Two of the WDs shown in Table 1 have negative progenitor lifetimes. This is due to the WD cooling age of these stars being larger than the cluster age. For WD17, we artificially set its initial mass to $7 M_\odot$ (the most massive star that produces a WD in the Ventura et al. 1998 models). For WD15, we compute a 95% confidence lower limit of 408 Myr for t_{cool} and determine the initial mass based on this cooling age. These stars are both plotted with open circles and an arrow pointing to higher masses to reflect the lower limits. It is unlikely that these objects are field WDs given their unusually high masses (see Madej, Nalezyty, & Althaus 2004 for field WD mass distribution).

Figure 3 (top) shows that, with just one star cluster, we have nearly doubled the number of data points on the initial-final mass plane. This is remarkable considering the time and effort required to establish the previous constraints (shown as triangles). Furthermore, half of our data points sit along a very tight sequence with initial masses in the range $2.8\text{--}3.4 M_\odot$ and final masses in the range $0.7\text{--}0.9 M_\odot$. Fitting these data points and their

TABLE 1
 DERIVED PARAMETERS OF WDS

Star	α (J2000)	δ (J2000)	T_{eff} (K)	$\log(g)$	M_f (M_{\odot})	M_V (theory)	M_V (obs.)	t_{cool} (Myr)	t_{ms} (Myr)	M_i (M_{\odot})
WD1	05:52:26.46	32:30:47.9	16500 ± 800	7.75 ± 0.19	0.48 ± 0.09	10.72	11.07	111 ± 32	539 ± 32	$2.79^{+0.05}_{-0.06}$
WD2	05:52:17.16	32:29:04.1	19900 ± 900	8.11 ± 0.16	0.69 ± 0.10	10.90	11.20	108 ± 36	542 ± 36	$2.76^{+0.08}_{-0.07}$
WD3	05:52:36.25	32:32:51.5	18300 ± 900	8.23 ± 0.21	0.76 ± 0.13	11.21	11.39	179 ± 64	471 ± 64	$2.92^{+0.16}_{-0.14}$
WD4	05:52:34.53	32:29:12.4	16900 ± 1100	8.40 ± 0.26	0.87 ± 0.15	11.65	11.51	329 ± 133	321 ± 133	$3.36^{+0.76}_{-0.40}$
WD5	05:52:25.11	32:30:55.7	18300 ± 1000	8.33 ± 0.22	0.83 ± 0.14	11.39	11.62	224 ± 85	426 ± 85	$3.02^{+0.26}_{-0.19}$
WD6*	05:52:18.08	32:29:38.4	17200 ± 1600	...	0.92 ± 0.15	11.76	11.76	300 ± 100	350 ± 100	$3.25^{+0.44}_{-0.28}$
WD7	05:52:36.96	32:33:29.9	17800 ± 1400	8.42 ± 0.32	0.88 ± 0.19	11.58	11.82	303 ± 148	347 ± 148	$3.26^{+0.78}_{-0.40}$
WD9	05:52:25.14	32:40:03.6	15300 ± 400	8.00 ± 0.08	0.61 ± 0.05	11.20	11.19	202 ± 28	448 ± 28	$2.97^{+0.06}_{-0.07}$
WD10	05:52:25.82	32:36:03.8	19300 ± 400	8.20 ± 0.07	0.74 ± 0.04	11.08	11.20	131 ± 19	519 ± 19	$2.81^{+0.04}_{-0.02}$
WD11	05:52:26.57	32:35:25.4	23000 ± 600	8.54 ± 0.10	0.96 ± 0.06	11.34	11.25	153 ± 30	498 ± 30	$2.86^{+0.07}_{-0.07}$
WD12	05:52:11.96	32:40:39.5	13300 ± 1000	7.91 ± 0.12	0.55 ± 0.07	11.34	11.45	313 ± 70	337 ± 70	$3.30^{+0.30}_{-0.22}$
WD13	05:52:16.21	32:38:18.5	18200 ± 400	8.27 ± 0.08	0.79 ± 0.05	11.30	11.46	183 ± 28	467 ± 28	$2.93^{+0.06}_{-0.07}$
WD14	05:52:06.43	32:38:29.4	11400 ± 200	7.73 ± 0.16	0.45 ± 0.08	11.38	11.55	318 ± 61	332 ± 61	$3.31^{+0.26}_{-0.20}$
WD15**	05:52:27.42	32:35:50.0	11300 ± 200	8.35 ± 0.15	0.83 ± 0.09	12.30	11.85	786 ± 189	... \pm ...	> 3.73
WD16	05:52:22.89	32:36:29.4	13100 ± 500	8.34 ± 0.10	0.83 ± 0.06	11.97	11.86	542 ± 94	108 ± 94	$5.20^{+?}_{-1.20}$
WD17**	05:52:29.29	32:37:06.7	12300 ± 400	8.72 ± 0.10	1.05 ± 0.05	12.77	12.16	1346 ± 256	... \pm ...	> 7
WD21*	05:52:26.42	32:30:04.3	17200 ± 2000	...	0.85 ± 0.15	11.59	11.59	261 ± 100	389 ± 100	$3.13^{+0.36}_{-0.25}$
WD24	05:52:25.34	32:29:35.2	18700 ± 1100	8.82 ± 0.24	1.11 ± 0.13	12.24	11.84	492 ± 237	158 ± 237	$4.43^{+?}_{-1.32}$

*Masses for these two WDs are determined by assuming they are cluster members - see §4.

**The cooling time for these two WDs (t_{cool}) is larger than the cluster age - see §4.

two dimensional errors to a straight line, we determine a slope of 0.33 and an intercept of -0.19. The residual rms of the fit is 0.03. This suggests that stars with masses between 2.8 and 3.4 M_{\odot} , and metallicities slightly less than solar, will lose 70–75% of their mass through stellar evolution.

Four of our stars are seen well below the tight sequence of points discussed above. Although only one of these four stars has an inconsistent theoretical magnitude, they could still be field WDs located near the cluster. Not only are their masses consistent with the distribution of field WDs ($M = 0.56 M_{\odot}$ - Sloan Digital Sky Survey data; Madej, Nalezyty, & Althaus 2004), but we also expect 4-5 WDs in our sample to be field stars based on WD number counts in blank fields surrounding NGC 2099 (Kalirai et al. 2001a). The lower masses of these stars could also be attributed to binary star evolution and mass transfer. We will investigate these possibilities further in J. S. Kalirai et al. (2005, in preparation).

We have plotted several theoretical and semi empirical relations in Figure 3. The dotted line is the revised semi empirical initial-final mass relationship from Weidemann (2000). The dashed line is the theoretical initial-final mass relationship from the Padova group stellar evolution models (Girardi et al. 2000; L. Girardi 2004, private communication) for $Z = 0.008$. The two solid lines are theoretical initial-final mass relations from Marigo (2001), for $Z = 0.008$ (top) and $Z = 0.02$ (bottom). The latter models have improved mass-loss mechanisms in their post-main sequence evolutionary phases and therefore should be preferred over the others (L. Girardi 2004, private communication). Considering this, it is interesting to note that half of our NGC 2099 cluster WDs reside in a region of the initial-final mass relationship bound by the two Marigo (2001) relations (see bottom

panel of Figure 3). This is what we would expect, given that the cluster metallicity falls between that used in the two models ($Z = 0.011$). We point out, however, that the errors in our measurements are too large for us to be able to discriminate between the two relations. Our data points are, however, mostly located above the other previous constraints. This can also be explained by the fact that almost all of the other clusters are solar or higher metallicity, resulting in more efficient mass loss during stellar evolution (Marigo 2001). Although this could be a systematic effect (e.g., the masses of the WDs in other clusters have been derived using different models), these results may be suggesting that, for the first time, we are seeing the effects of metallicity on the initial-final mass relationship. In J. S. Kalirai et al. (2005, in preparation), we will eliminate these systematics by reevaluating all of the previous data on the initial-final mass relation (including the new results of Williams, Bolte, & Koester 2004) using a consistent fitting method and set of evolutionary models.

The spectroscopic measurement of masses of WDs with $V \simeq 23$ has not been previously accomplished. The number of targets that are accessible at these magnitudes is several orders of magnitudes larger than previously identified (see work on the on-going *CFHT* Open Star Cluster Survey; Kalirai et al. 2001a; 2001b; 2001c; 2003). With continuing observations of rich open star clusters, we can envision placing >100 data points into this very fundamental relation. By observing both younger and older clusters, the entire initial progenitor mass range can be constrained and a detailed initial-final mass relation can be produced.

We would like to thank Pierre Bergeron for providing us with his models and spectral fitting routines. This project could not have succeeded without this input. We also wish to thank Dan Kelson, Inger Jorgenson, and Jarrod Hurley for providing help with various parts of this project. J. S. K. received financial support during this work through an NSERC PGS-B research grant. The

research of H. B. R. is supported in part by NSERC. B. M. S. H. is supported by NASA grant ATP03-0000-0084. B. K. G. acknowledges the financial support of the Australian Research Council. T. v. H. appreciatively acknowledges support from NASA through LTSA grant NAG5-13070.

REFERENCES

- Bergeron, P., Saffer, R. A., & Liebert, J. 1992, *ApJ*, 394, 228
 Claver, C. F. et al. 2001, *ApJ*, 563, 987
 Fontaine, G., Brassard, P., & Bergeron, P. 2001, *PASP*, 113, 409
 Fusi-Pecci, F. & Renzini, A. 1976, *A&A* 46, 447
 Girardi, L. et al. 2000, *A&AS*, 141, 371
 Hansen et al. 2004, accepted in *ApJS*, astro-ph/0401443
 Hurley, J. R., Pols, O. R., & Tout, C. A. 2000, *MNRAS*, 315, 543
 Jeffries, R. D. 1997, *MNRAS*, 288, 585
 Kalirai, J. S. et al. 2005, submitted to *ApJL*
 Kalirai, J. S. et al. 2003, *AJ*, 126, 1402
 Kalirai, J. S. et al. 2001a, *AJ*, 122, 3239
 Kalirai, J. S. et al. 2001b, *AJ*, 122, 266
 Kalirai, J. S. et al. 2001c, *AJ*, 122, 257
 Kelson, D. 2003, *PASP*, 115, 808, 688
 Koester, D. & Reimers, D. 1996, *A&A*, 313, 810
 Koester, D. & Reimers, D. 1993, *A&A*, 275, 479
 Koester, D. & Reimers, D. 1985, *A&A*, 153, 260
 Koester, D. & Reimers, D. 1981, *A&A*, 99, L8
 Madej, J., Nalezyty, M., & Althaus, L. G. 2004, *A&A*, 419, L5
 Marigo, P. 2001, *A&A*, 370, 194
 Murowinski, R. et al. 2003, 2003, *SPIE*, 4841, 1440
 Oke, J. B. 1995, *PASP*, 107, 375
 Press, W. H. et al. 1986, *Numerical Recipes*, Cambridge: Cambridge Univ. Press
 Reimers, D. & Koester, D. 1994, *A&A*, 285, 451
 Reimers, D. & Koester, D. 1989, *A&A*, 218, 118
 Reimers, D. & Koester, D. 1982, *A&A*, 116, 2, 341
 Somerville, R. S. & Primack, J. R. 1999, *MNRAS*, 310, 1087
 van den Bergh, S. & Tammann, G. 1991, *ARA&A*, 29, 363
 Ventura, P. et al. 1998, *A&A*, 334, 953
 Weidemann, V. 2000, *A&A*, 363, 647
 Weidemann, V. 1987, *A&A*, 188, 74
 Weidemann, V. & Koester, D. 1983, *A&A*, 121, 77
 Weidemann, V. 1977, *A&A*, 59, 411
 Williams, K. A., Bolte, M., & Koester, D. 2004, *ApJ*, 615, L49
 Yi, S. et al. 2001, *ApJS*, 136, 417